REVISTA Mundi
Engenharia, Tecnologia e Gestão
INSTITUTO FEDERAL Paraná

Model Reference Control Applied on the Velocity Tracking of a Welding Robot

Controle por Modelo de Referência Aplicado ao Rastreamento de Velocidade de um Robô Soldador

Andreyna Sárila Ramos Ferreira[1]

Débora Debiaze de Paula[2]

Paulo Jefferson Dias de Oliveira Evald[3]

Rodrigo Zelir Azzolin[4]

Abstract: Robotics has been expanding over last decades, employed mainly to the activities that are most harmful to human beings. Considering that welding is one of the most risky activities in industries, studies and researches in the process automation are quite important. In this context, this work contributes to the control of the velocity tracking of the displacement of a linear welding robot. The mathematical modelling of the robot is presented, and the chosen control technique is Model Reference Control, which allows project controller based on the desired behaviour for the robot. To corroborate controller effectiveness, simulation and experimental results are presented and discussed, proving that proposed technique is adequate to control the robot velocity.

***Keywords*:** Model Reference Control. Welding Robot. Velocity Control.

Resumo: A robótica vem se expandindo ao longo dos anos, sendo principalmente aplicada nas atividades mais danosas aos seres humanos. Considerando que a soldagem é uma das atividades de maior risco nas indústrias, estudos e pesquisas na automação deste processo são extremamente importantes. Neste contexto, este trabalho traz uma contribuição para o controle do rastreamento de velocidade de deslocamento de um robô soldador. A modelagem matemática do robô é apresentada, e a técnica utilizada é o Controle por Modelo de Referência, pois permite a escolha do exato comportamento desejado do robô. Para provar a eficácia do controlador, resultados de simulação e experimentais são apresentados e discutidos, provando que a técnica é adequada para controlar a velocidade do robô, levando-o à referência.

***Palavras-chave*:** Controle por Modelo de Referência. Robô Soldador. Controle de Velocidade.

[1]Engenheira, Instituto Tecnológico de Aeronáutica (ITA) e andreynasrf@gmail.com.
[2]Engenheira, Universidade Federal do Rio Grande (FURG) e deboradebiaze@gmail.com.
[3]Doutor, Universidade Franciscana (UFN) e paulo.evald@gmail.com.
[4]Doutor, Universidade Federal de Rio Grande (FURG) e rodrigoazzolin@gmail.com.

Revista Mundi, Engenharia e Gestão, Paranaguá, PR, v. 6, n. 4, p. 374-01, 374-24, 2021.
DOI: 10.21575/25254782rmetg2021vol6n41464

1 Introduction

Robotics has expanded widely in recent years (DECANIO, 2016; DECKER; FISCHER; OTT, 2017), being a key solution for activities that expose human to dangerous situations. One of the industrial activities that most causes damage to operators is welding processes (MISTRY, 2015; SINGH; CHADHA, 2016; MARK et al., 2015) and, therefore, currently, is the area that concentrate most industrial robots. Inherently, the robots control is a growing field of research to improve better results with this industrial robots.

Often, the industrial robots are modular, which turn easier their transport and assembly, sparks replacement, instrumentation, corrective maintenance and other advantages. One of these modules is responsible for robots moving. The main control parameter intrinsic to this module is the sewing speed, which influences the appearance of the weld bead and determine thermal input in the welded joints (MENDES et al., 2016; CORREIA et al., 2016), affecting directly the weld bead quality. Different welding techniques require different velocities, and variations in it can result in weld beads flaws, such as bubbles, cracks, among other discontinuities (ÜNEL; TABAN, 2017; NATHAN et al., 2015).

In the literature, there are some works dedicated to the robot control with aim to improve welding bead quality. Among them, some interesting works are (CHEN et al., 2015), where was proposed a feedback control system to assist the welder in regulating his/her arm movement in real time to achieve the desired torch travel speed. The results presented improvements on weld bead quality, however, to perform it, a visual-based system was required. Besides, on (LIU; ZHANG, 2017) was proposed an intelligent algorithm to fuse the welder intelligence to the robot velocity controller. In that work, a fuzzy system was responsible to switch the robot guidance between operator and robot controller. The results shown the effectiveness of algorithm, however, its main drawback is the need of a relevant capacity processing microcontroller. In other way, to increase the stability of welding speed and smoothness of the weld track, on (YUXIANG; DONG; JILUAN, 2019), a seam-tracking based on dynamic trajectory planning for a mobile welding robot was presented. To implement it, a front-placed laser-based vision sensor was utilised to extract weld seam location, besides trend and direction of the weld line. With it, a closed-loop control system adjust automatically robot dynamics. Again, an dedicated apparatus is required to execute it experimentally.

Considering these facts, this work contributes to the control research area for linear welding robots. Here, it presented the detailed design of a velocity tracking

Revista Mundi, Engenharia e Gestão, Paranaguá, PR, v. 6, n. 4, p. 374-01, 374-24, 2021.
DOI: 10.21575/25254782rmetg2021vol6n41464

controller, which does not require additional hardware, or high processing capacity microcontroller, and apply it on a welding robot, a *Bug-O Modular Drive System*. The proposed control strategy is Model Reference Control (MRC), which allow the designer to define exactly the desired behaviour for the controlled system.

The organisation of this work is given as follows: in Section 2, the welding robot is presented, as well as its mathematical model, focused on robot's displacement module. Next, on Section 3, it is presented the theory and design of applied control strategy. Besides, in Section 4, simulation results are presented and discussed. To analyse controller performance, two situations are considered: one with reference application only, and other, also with reference tracking, but adding disturbances, parametric variations, as well as process and measurement noises. Finally, on Section 5, the experimental results are presented and discussed. The final considerations about the developed work are made in Section 6.

2 Welding Robot *Bug-O MDS*

The *Bug-O Modular Drive System Linear Weaver*, used as platform in this project, produces linear cuts and welds. In addition to the longitudinal movement over rail, the robot allows welding torch movement on transverse direction of displacement, by an oscillatory motion, which gives two degrees of freedom. In practice, the robot moves on a linear rail, fixed through metallic structures parallel to the welding chamfer; loads welding torch, following the chamfer and executing swinging weld seam. Figure 1 shows the robot, in its original configuration, being used in a GMAW (Gas Metal Arc Welding) process.

The robot is a modular system, that is, its displacement over rail and displacement of its arm for fixing the welding torch are independent movements. Thus, this robot consists of two main modules: the displacement module over rail (*tractor*) and the sewing module (*weaver*), which carries the torch. This system format is conducive to the industrial environment, as it facilitates purchase of new modules, in case of damage, besides, it making transportation faster. They give shelter to the robot motors, allowing its movement and control. In this work, the focus will be on module that allows the robot to move over rail, called *tractor*.

The *tractor* has high torque, low inertia motor for precise stops and starts, which has an operating voltage of -15 to $15\,V$. It also has a safety brake of power, three times greater than that of stopping and starting the engine. Furthermore, it is equipped

Revista Mundi, Engenharia e Gestão, Paranaguá, PR, v. 6, n. 4, p. 374-01, 374-24, 2021.
DOI: 10.21575/25254782rmetg2021vol6n41464

Figure 1: Welding robot *Bug-O Modular Drive System Linear Weaver*

Source: adapted from (BUG-O SYSTEMS CORPORATION, 2019a)

with motor overload protection that stops the engine and engages brake whenever an excessive load is placed on the machine, having a vertical load capacity equal to $27\,kg$ and horizontal to $45\,kg$. A schematic of the *tractor* module is presented on Figure 2, as well as indications of the control module and rail base. It is emphasised that control module is not used in this work, since a microcontroller is used to operate the motors.

Figure 2: Constituent parts of the robot *Bug-O MDS tractor* module

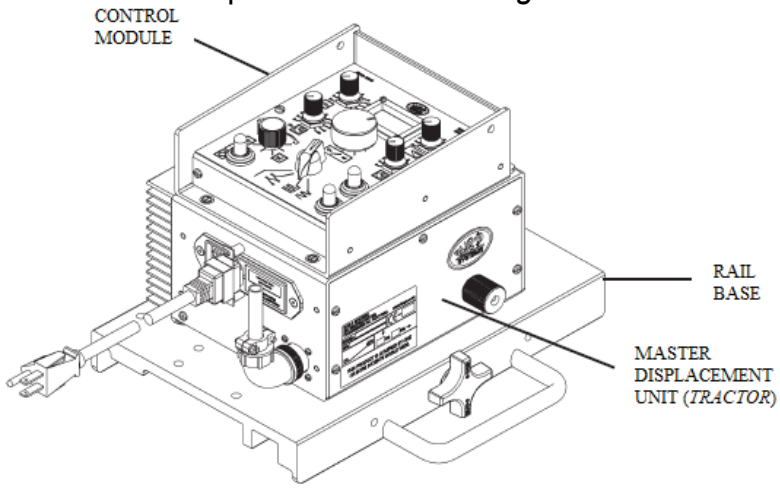

Source: adapted from (BUG-O SYSTEMS CORPORATION, 2019b)

Revista Mundi, Engenharia e Gestão, Paranaguá, PR, v. 6, n. 4, p. 374-01, 374-24, 2021.
DOI: 10.21575/25254782rmetg2021vol6n41464

2.1 Mathematical model of the *tractor* module

The modelling of the robot's *tractor* module includes forces resulting from relationship between motor, gearbox and rack, in addition to the dynamics of motor itself. The motor responsible for longitudinal movement of the welding robot is a pancake-type motor. However, its model was approximated to a DC motor model, due to its high dynamics similarity. The Figure 3 presents a block diagram of the system. As modelling has an extensive mathematical development, it is here omitted. Further details of this modelling, including engine, gearbox, rack and inclination of the welding plate dynamics, can be checked on (FERREIRA et al., 2020).

Figure 3: Block diagram of the *tractor* module system

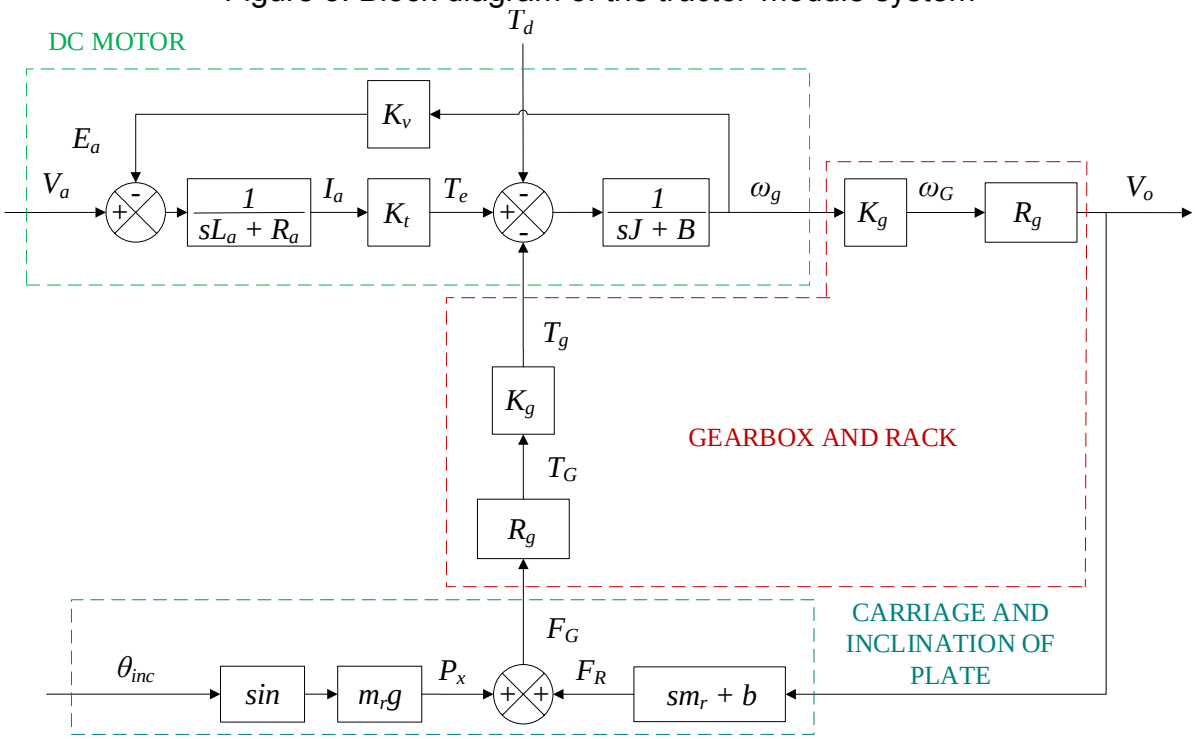

Source: From authors (2021)

where s is the complex variable in the frequency domain and the variables on Figure 3 are:

Gearbox and rack

K_g	Gearbox gain	$[-]$;
R_g	Gear radius on the rack	$[mm]$;
T_g	Load torque on the high speed shaft	$[N]$;
T_G	Load torque on the low speed shaft	$[N]$;
ω_G	Angular speed on the low rotation axis	$[rad/s]$;

Revista Mundi, Engenharia e Gestão, Paranaguá, PR, v. 6, n. 4, p. 374-01, 374-24, 2021.
DOI: 10.21575/25254782rmetg2021vol6n41464

DC Motor

B	Motor shaft mechanical friction coefficient	$\left[\frac{(kg\,m)}{(rad^2\,s)}\right]$;
E_a	Counter-electromotive voltage generated in the armature	[V];
I_a	Armature current	[A];
J	Moment of inertia	[$kg\,m^2$];
K_t	Torque constant of the motor	[$(N\,m)/A$];
K_v	Voltage constant of the motor	[$(N\,m)/A$];
L_a	Armature winding inductance	[H];
R_a	Armature winding resistance	[Ω];
T_d	Disturbance torque on the high rotation shaft	[N];
T_e	Electromagnetic torque on the high rotation shaft	[N];
V_a	Armature voltage at the motor terminals	[V];
ω_g	Angular velocity on the high rotation shaft	[rad/s];

Carriage and inclination of plate

b	Coefficient of viscous friction of the wheel bearings	[kg/s];
F_G	Force developed by the relationship between gear and rack	[N];
F_R	Resulting force of the system	[N];
g	Gravity acceleration	[m/s^2];
m_r	Robot mass, considering both *tractor* and *weaver* modules	[kg];
P_x	Decomposition, on the *x* axis, of the P weight force	[N];
Θ_{inc}	Inclination angle of the *tractor* module	[°].

After defining the system model, tests and experiments were carried out to identify the electrical and mechanical parameters of the robot. The DC motor parameters (R_a, L_a, B, J, K_t and K_v) were identified from blocked rotor test, which consisted on applying voltage steps at motor terminals and measuring armature voltage, armature current, angular speed and constant speed decay time. From these information, it was possible to calculate the required parameters. Finally, the voltage constant was identified through relationship between mechanical and electrical powers. Furthermore, mechanised welding systems parameters (m_r, b, K_g and R_g) were identified as follows. The system mass was determined by weighing and wheel bearings' viscous friction coefficient was identified applying a voltage step to the motor and obtaining the velocity time constant, which was compared to a standard first order transfer function. Besides, the gearbox gain was extracted from robot's manual and gear radius was measured using a tape measure. Table 1 shows all identified parameters.

Revista Mundi, Engenharia e Gestão, Paranaguá, PR, v. 6, n. 4, p. 374-01, 374-24, 2021.
DOI: 10.21575/25254782rmetg2021vol6n41464

Table 1: Identified plant parameters

DC Motor			
Symbol	**Value**	**Standard deviation**	**Unit**
R_a	4.910	3.348e-01	Ω
L_a	13.300e-03	–	H
B	1.278e-04	–	$kg\,m^2/(rad^2\,s)$
J	8e-05	7.235e-06	$kg\,m^2$
K_t	3.423e-02	8.040e-03	$N\,m/A$
K_v	3.423e-02	8.040e-03	$N\,m/A$
Robot			
Symbol	**Value**		**Unit**
m_r	11.10		kg
b	46.44		kg/s
K_g	1/60		–
R_g	0.008		m

Source: From authors (2021)

The transfer function (TF) of the *tractor* module, $G(s)$, is given by

$$G(s) = \frac{V_o(s)}{V_a(s)} = \frac{b_0}{a_0\,s^2 + a_1\,s + a_2}, \tag{1}$$

where V_o is the linear velocity of robot displacement over rail and V_a is the armature voltage applied to the motor terminals. Besides, TF coefficients are:

$$\begin{aligned} b_0 &= K_{g_t} R_{eng_t} K_{t_t}; \\ a_0 &= L_{a_t}[J_t + (K_{g_t} R_{eng_t})^2 m_r]; \\ a_1 &= L_{a_t} B_t + R_{a_t} J_t + (L_{a_t} b_t + R_{a_t} m_r)(K_{g_t} R_{eng_t})^2; \\ a_2 &= R_{a_t}[B_t + (K_{g_t} R_{eng_t})^2 b_t] + K_{v_t} K_{t_t}. \end{aligned} \tag{2}$$

With identified parameters, the plant TF is

$$G(s) = \frac{4.28}{s^2 + 370.8\,s + 1690.6}, \tag{3}$$

which on State Space (SS) is represented by

$$\boldsymbol{A} = \begin{bmatrix} -370.80 & -1690.60 \\ 1 & 0 \end{bmatrix}, \quad \boldsymbol{B} = \begin{bmatrix} 1 \\ 0 \end{bmatrix}, \quad \boldsymbol{C} = \begin{bmatrix} 0 & 4.28 \end{bmatrix} \quad \text{and} \quad \boldsymbol{D} = [0]. \tag{4}$$

This model was validated through simulations and experiments carried out on the

Revista Mundi, Engenharia e Gestão, Paranaguá, PR, v. 6, n. 4, p. 374-01, 374-24, 2021.
DOI: 10.21575/25254782rmetg2021vol6n41464

robot. For these tests, disturbance torque and inclination angle were considered nulls. Moreover, the experiments were carried out with the *tractor* module attached to the rail, as considered on model.

3 Model Reference Control

The MRC is a control technique, whose objective is to modify the dynamics of the controlled system in order to make its behaviour equivalent to a desired reference system. Next, the technique will be explained mathematically according to (IOANNOU; SUN, 1996).

Let be a linear and time invariant (LTI) system, with single-input and single-output (SISO), described by the differential equations:

$$\dot{x}_p = \boldsymbol{A}_p\, \boldsymbol{x}_p + \boldsymbol{B}_p\, u_p \quad \text{and} \quad y_p = \boldsymbol{C}_p\, \boldsymbol{x}_p, \tag{5}$$

where:

$\boldsymbol{x}_p$	Plant state variables vector, being $\boldsymbol{x}_p \in \Re^n$;
y_p	Plant output sign, being $y_p \in \Re^1$;
u_p	Plant input sign, being $u_p \in \Re^1$;
$\boldsymbol{A}_p$, $\boldsymbol{B}_p$ and $\boldsymbol{C}_p$	Matrices representing the plant in SS with adequate order.

In this way, the TF of the plant is given by:

$$\frac{y_p}{u_p} = G_p(s), \tag{6}$$

being $G_p(s)$ described as

$$G_p(s) = k_p\, \frac{Z_p(s)}{R_p(s)}, \tag{7}$$

where

$G_p(s)$	Plant transfer function;
k_p	Plant high frequency gain;
Z_p and R_p	Plant monic polynomials.

The reference model is chosen by the controller designer according to the desired parameters for the plant, which are: damping coefficient (ζ) and natural frequency (ω_n).

Revista Mundi, Engenharia e Gestão, Paranaguá, PR, v. 6, n. 4, p. 374-01, 374-24, 2021.
DOI: 10.21575/25254782rmetg2021vol6n41464

Therefore, the reference model is described by the following differential equations:

$$\begin{aligned} \dot{x_m} &= \boldsymbol{A}_m \boldsymbol{x}_m + \boldsymbol{B}_m r \quad \text{and} \\ y_m &= \boldsymbol{C}_m \boldsymbol{x}_m, \end{aligned} \tag{8}$$

where

$\boldsymbol{x}_m$	Reference model state variables vector;
$\boldsymbol{y}_m$	Reference model output sign;
r	Reference input signal;
$\boldsymbol{A}_m$, $\boldsymbol{B}_m$, $\boldsymbol{C}_m$	Matrices representing the reference model in SS with adequate order.

In this way, the TF of the reference model is given by:

$$\frac{y_m}{r} = G_m(s), \tag{9}$$

being $G_m(s)$ described as

$$G_m(s) = k_m \frac{Z_m(s)}{R_m(s)}, \tag{10}$$

where:

$G_m(s)$	Reference model transfer function ;
k_m	Reference model gain;
Z_m and R_m	Reference model monic polynomials.

With plant and model presented, the problem of MRC is to determine the plant input u_p so that all signals are limited and plant output y_p tracks as much as possible the given reference input r. In order to design an implementable control law to be defined, without differentiation and consisting only of measured signals, some assumptions for plant and reference model are assumed.

Plant assumptions:

1. $Z_p(s)$ is a *Hurwitz* monic polynomial of m_p degree;
2. There is an upper limit n for the n_p degree of $R_p(s)$;
3. The relative degree of the $G_p(s)$ plant is $n^* = n_p - m_p$;
4. The k_p high frequency gain signal is known.

Revista Mundi, Engenharia e Gestão, Paranaguá, PR, v. 6, n. 4, p. 374-01, 374-24, 2021.
DOI: 10.21575/25254782rmetg2021vol6n41464

Reference model assumptions:

1. $Z_m(s)$ and $R_m(s)$ are *Hurwitz* monic polynomial of q_m and p_m degrees, respectively, where $p_m \leq n$;

2. The relative degree of the reference model $G_m(s)$ is $n^*_m = p_m - q_m$, equal to relative degree of the plant $G_p(s)$.

In this way, the objective of the MRC is achieved if the control law u_p is chosen so that the closed-loop transfer function has stable poles and is equal to $G_m(s)$. This correspondence is what guarantees that, for any reference input signal r, the plant output y_p converges to the reference model output y_m exponentially.

If the plant is known and does not have cancellations of poles and zeros, a choice for u_p is the open loop control law. Equating y_p to y_m, it is defined:

$$G_p(s)\, u_p = G_m(s)\, r, \tag{11}$$

which results in:

$$u_p = C(s)\, r, \tag{12}$$

being

$$C(s) = \frac{k_m}{k_p}\, \frac{Z_m(s)}{R_m(s)}\, \frac{R_p(s)}{Z_p(s)}. \tag{13}$$

Replacing (6) and (7) in (12), it is defined as

$$\frac{y_p}{r} = \frac{k_m}{k_p}\, \frac{Z_m(s)}{R_m(s)}\, \frac{R_p(s)}{Z_p(s)}\, \frac{k_p\, Z_p}{R_p}. \tag{14}$$

This transfer function is equivalent to the transfer function of the reference model, $G_m(s)$.

If the plant has parametric variations, these variations will result in imperfect cancellations of zeros and poles. In addition, it can lead the intermediate states to instability due to initial non-zero conditions. Thus, in this case, it can be used an alternative control law, illustrated in Figure 4, and mathematically described by

$$u_p = \theta_1^{*T}\, \frac{\alpha(s)}{\Lambda(s)}\, u_p + \theta_2^{*T}\, \frac{\alpha(s)}{\Lambda(s)}\, y_p + \theta_3^*\, y_p + c_0^*\, r, \tag{15}$$

Revista Mundi, Engenharia e Gestão, Paranaguá, PR, v. 6, n. 4, p. 374-01, 374-24, 2021.
DOI: 10.21575/25254782rmetg2021vol6n41464

being

$$\alpha(s) \triangleq \alpha_{n-2}(s) = [s^{n-2}, s^{n-3}, ..., s, 1]^T \quad \text{for} \quad n \geq 2 \quad \text{and} \quad \alpha(s) \triangleq 0 \quad \text{for} \quad n = 1, \tag{16}$$

where

$\alpha(s)$	Constant matrix to be projected;
c_0^*	Constant parameter to be projected, being $c_0^* \in \Re^1$;
θ_1^*, θ_2^*, θ_3^*	Constant parameters to be projected, being θ_1^* and $\theta_2^* \in \Re^{n-1}$, and $\theta_3^* \in \Re^1$;
$\Lambda(s)$	*Hurwitz* monic polynomial arbitrary of $n-1$ degree that contains $Z_m(s)$ as a factor.

Figure 4: Structure of the Model Reference Control

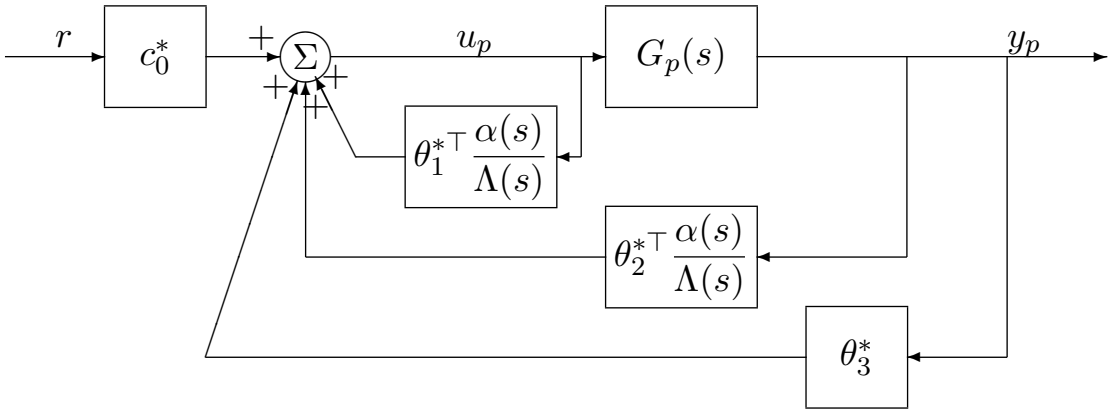

Source: adapted from (IOANNOU; SUN, 1996)

The $\Lambda(s)$ polynomial is defined as

$$\Lambda(s) = \Lambda_0(s)\, Z_m(s), \tag{17}$$

where

$\Lambda_0(s)$	*Hurwitz* monic polynomial of $n_0 = n - 1 - q_m$ degree .

It is emphasised that the $\Lambda_0(s)$ polynomial is chosen in order to satisfy (17). Besides, the controller parameters vector is

$$\theta^* = [\ \theta_1^{*T}, \theta_2^{*T}, \theta_3^*, c_0^*\ ]^T \in \Re^{2n}, \tag{18}$$

this being defined so that the transfer function from r to y_p is equal to $G_m(s)$.

Revista Mundi, Engenharia e Gestão, Paranaguá, PR, v. 6, n. 4, p. 374-01, 374-24, 2021.
DOI: 10.21575/25254782rmetg2021vol6n41464

The plant transfer function shown on Figure 4 is defined as

$$y_p = G_c(s)\, r, \tag{19}$$

being

$$G_c(s) = \frac{c_0^*\, k_p\, Z_p\, \Lambda^2}{\Lambda[(\Lambda - \theta_1^{*T}\, \alpha(s))\, R_p - k_p\, Z_p(\theta_2^{*T}\, \alpha(s) + \theta_3^{*T}\, \Lambda)]}. \tag{20}$$

The control objective is satisfied when the controller parameters are such that closed-loop poles are stable and $G_c(s) = G_m(s)$, with such conditions being met for all $s \in C$.

If $G_c(s) = G_m(s)$, then

$$\frac{c_0^*\, k_p\, Z_p\, \Lambda^2}{\Lambda[\ (\Lambda - \theta_1^{*T}\, \alpha(s))\, R_p - k_p\, Z_p(\theta_2^{*T}\, \alpha(s) + \theta_3^{*T}\, \Lambda)\ ]} = K_m\, \frac{Z_m(s)}{R_m(s)}. \tag{21}$$

Defining

$$c_0^* = \frac{k_m}{k_p}, \tag{22}$$

and replacing (17) in (21), it is calculated as

$$(\Lambda - \theta_1^{*T}\, \alpha)\, R_p - k_p\, Z_p(\theta_2^{*T}\, \alpha + \theta_3^{*T}\, \Lambda) = Z_p\, \Lambda_0\, R_m. \tag{23}$$

Performing the manipulation of the equation, it results in

$$\theta_1^{*T}\, \alpha(s)\, R_p(s) + k_p\, (\theta_2^{*T}\, \alpha(s) + \theta_3^{*T}\, \Lambda(s))\, Z_p(s) = \Lambda(s)\, R_p(s) - Z_p(s)\, \Lambda_0(s)\, R_m(s). \tag{24}$$

Isolating the coefficients with *s* on both sides of (24), this equation can be expressed algebraically as

$$S\, \bar{\theta}^* = p, \tag{25}$$

where

- S Matrix of dimensions $(n + n_p - 1)$x$(2\, n - 1)$, dependent on the coefficients of R_p, $k_p\, Z_p$ and Λ;
- $\bar{\theta}^*$ Parameters vector θ^*, being $\bar{\theta}^* = [\theta_1^{*T}, \theta_2^{*T}, \theta_3^*]^T$;
- p Vector of dimensions $(n + n_p - 1)$x1, dependent on the coefficients of $\Lambda\, R_p - Z_p\, \Lambda_0\, R_m$.

Thus, starting from (25), the $\bar{\theta}^*$ vector is defined, completing the necessary parameters for controller project.

Revista Mundi, Engenharia e Gestão, Paranaguá, PR, v. 6, n. 4, p. 374-01, 374-24, 2021.
DOI: 10.21575/25254782rmetg2021vol6n41464

As aforementioned, (15) ensures that closed-loop transfer function $G_c(s)$ of the plant has all stable poles, and that $G_c(s) = G_m(s)$. In the approached analysis, initial conditions of the plant, reference model and filters were assumed as zero. These assumptions are common in most control projects for LTI systems, and is valid as long as any cancellation of poles or zeros in the closed-loop plant occurs on the left side of *s*-plane of $C(s)$ (C^-). In another case, non-null initial conditions can lead to unlimited internal states that correspond to cancellations of zeros and poles on the right side of *s*-plane of $C(s)$ (C^+).

In this controller design, all cancellations in $G_c(s)$ are guaranteed to occur in C^-, assuming stable zeros for the plant transfer function and using stable filters on control law. The analysis of the effect of initial conditions can be done through representations of plant, reference model and controller at SS. Initially, the control law, expressed as (15), can be written as

$$u_p = \theta_1^{*T}\,\omega_1 + \theta_2^{*T}\,\omega_2 + \theta_3^{*}\,y_p + c_0^{*}\,r, \tag{26}$$

being the filters equal to

$$\omega_1 = \frac{\alpha(s)}{\Lambda(s)}\,u_p \quad \text{and} \quad \omega_2 = \frac{\alpha(s)}{\Lambda(s)}\,y_p, \tag{27}$$

where

$\boldsymbol{\omega}_1$, $\boldsymbol{\omega}_2$ Controller filters, with $\boldsymbol{\omega}_1$, $\boldsymbol{\omega}_2 \in \Re^{n-1}$.

Thus, replacing $\dfrac{\alpha(s)}{\Lambda(s)}$ in the filters, these equations in SS are given by

$$\begin{aligned} \dot{\boldsymbol{\omega}}_1 &= \boldsymbol{F}\,\boldsymbol{\omega}_1 + \boldsymbol{g}\,u_p \quad \text{and} \\ \dot{\boldsymbol{\omega}}_2 &= \boldsymbol{F}\,\boldsymbol{\omega}_2 + \boldsymbol{g}\,y_p, \end{aligned} \tag{28}$$

with $\omega_1(0) = \omega_2(0) = 0$, being

$$\boldsymbol{F} = \begin{bmatrix} -\lambda_{n-2} & -\lambda_{n-3} & -\lambda_{n-4} & ... & -\lambda_0 \\ 1 & 0 & 0 & ... & 0 \\ 0 & 1 & 0 & ... & 0 \\ \vdots & \vdots & \ddots & \ddots & \vdots \\ 0 & 0 & ... & 1 & 0 \end{bmatrix} \quad \text{e} \quad \boldsymbol{g} = \begin{bmatrix} 1 \\ 0 \\ \vdots \\ 0 \end{bmatrix}, \tag{29}$$

Revista Mundi, Engenharia e Gestão, Paranaguá, PR, v. 6, n. 4, p. 374-01, 374-24, 2021.
DOI: 10.21575/25254782rmetg2021vol6n41464

with λ_i equal to the coefficients of

$$\Lambda(s) = s^{n-1} + \lambda_{n-2}\, s^{n-2} + ... + \lambda_1\, s + \lambda_0 = det(s\, \boldsymbol{I} - \boldsymbol{F}), \tag{30}$$

where

$\boldsymbol{F}$, $\boldsymbol{g}$ Representation in SS of $\frac{\alpha(s)}{\Lambda(s)}$, that is, $det(s\, \boldsymbol{I} - \boldsymbol{F})\, \boldsymbol{g} = \frac{\alpha(s)}{\Lambda(s)}$.

In this way, the filters are designed and finally, the control law is defined in the SS as

$$u_p = \boldsymbol{\theta}^{*T}\, \boldsymbol{\omega}, \tag{31}$$

with $\boldsymbol{\theta}^* = [\ \theta_1^{*T}, \theta_2^{*T}, \theta_3^*, c_0^*\ ]^T$ and $\boldsymbol{\omega} = [\ \boldsymbol{\omega}_1^T, \boldsymbol{\omega}_2^T, y_p, r\ ]^T$. Figure 5 shows a block diagram of the closed-loop plant according to (28) and (31).

Figure 5: Block diagram of the closed-loop plant with the MRC control law

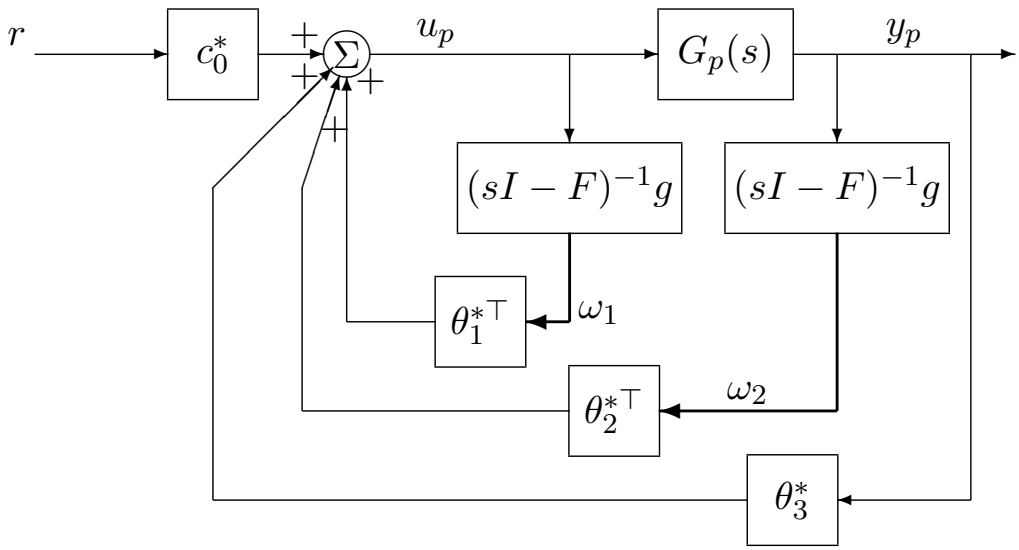

Source: adapted from (IOANNOU; SUN, 1996)

3.1 Controller Design

For MRC design, firstly the identified plant TF was set to standard TF representation, used on MRC theory. The *tractor* module TF is given by 3, then

$$\begin{aligned} &k_p = 4.28; \\ &Z_p(s) = 1 \quad \text{and} \\ &R_p(s) = s^2 + 370.8\, s + 1690.6. \end{aligned} \tag{32}$$

Revista Mundi, Engenharia e Gestão, Paranaguá, PR, v. 6, n. 4, p. 374-01, 374-24, 2021.
DOI: 10.21575/25254782rmetg2021vol6n41464

For the definition of the reference model TF, it is necessary to define performance criteria, which must be respected by controlled system. The welding robot, in its original structure, has a hardware PID controller along with the drive system, which is inaccessible. However, in this work, a low-cost drive system alternative was used, based on the electronic module IRAM (without hardware controller). Thus, aiming for a similar dynamics behaviour to that produced by robot with original controlled hardware, its response with a factory controller was first analysed. When applying a $30\,mm/s$ step, a time constant τ of $203\,ms$ and an accommodation time T_a (2 %) of $524\,ms$ were identified. Thus, the following performance criteria were defined: damping factor of $\zeta = 1$ and natural frequency of $\omega_n = 7,64\,rad/s$. Therefore, respecting the plant and reference model assumptions, the reference model TF is

$$G_m(s) = 58.27\frac{1}{s^2 + 15.27\,s + 58.27}, \tag{33}$$

being defined

$$\begin{aligned} &k_m = 58.27; \\ &Z_m(s) = 1 \quad \text{and} \\ &R_m(s) = s^2 + 15.27\,s + 58.27. \end{aligned} \tag{34}$$

The control law used in this project, which considers parametric variations, is presented on (15). Designing the controller for *tractor* module system, it starts by choosing $\Lambda_0(s)$ polynomial in order to satisfy (17). Knowing $Z_m(s)$ and that $\Lambda(s)$ must have $n-1$ degree, it is calculated as

$$\Lambda(s) = \Lambda_0(s) = s + 367. \tag{35}$$

As the $\Lambda(s)$ value determines $\boldsymbol{F}$ matrix of filters, the second term must be determined according to the desired response for system. In this choice, there must be a guarantee that high frequencies are not cut, so that reference value can be reached. Besides, it must also be guaranteed that plant is following the reference model.

According to (22) and knowing the values of model and plant gains, it is calculated its relation as

$$c_0^* = \frac{58.27}{4.28} = 13.61. \tag{36}$$

Revista Mundi, Engenharia e Gestão, Paranaguá, PR, v. 6, n. 4, p. 374-01, 374-24, 2021.
DOI: 10.21575/25254782rmetg2021vol6n41464

Considering the system parameters, and from (24), it is determined that

$$\begin{aligned}\theta_1^{*T}\,\alpha(s)\,R_p(s) + k_p\,(\theta_2^{*T}\,\alpha(s) + \theta_3^{*T}\,\Lambda(s))\,Z_p(s) &= \Lambda(s)\,R_p(s) - Z_p(s)\,\Lambda_0(s)\,R_m(s)\\ \theta_1^{*T}\,(s^2 + 370.8\,s + 1690.6) + 4,28\,[\theta_2^{*T} + \theta_3^{*T}\,(s+367)] &= \\ = (s+367)\,(s^2 + 370.8\,s + 1690.6) - (s+367)\,(s^2 + 15.27\,s + 58.27).&\end{aligned} \tag{37}$$

Isolating the coefficients with *s* on both sides, it is calculated

$$\begin{aligned}\theta_1^{*T}\,s^2 + (370.8\,\theta_1^{*T} + 4.28\,\theta_3^{*T})\,s + (1690.6\,\theta_1^{*T} + 4.28\,\theta_2^{*T} + 1570.76\theta_3^{*T}) &= \\ = 355.51\,s^2 + 132.11e(+3)\,s + 599.06e(+3)&\end{aligned} \tag{38}$$

Solving (38) in an algebraic way, the controller parameters vector is defined

$$\theta^* = \begin{bmatrix}355.51 & -25301.39 & 67.69\end{bmatrix}^T. \tag{39}$$

Knowing that $\Lambda(s)$ is equal to the polynomial presented in (35), the coefficients for the $\boldsymbol{F}$ definition are

$$\lambda_1 = 1 \quad \text{and} \quad \lambda_0 = 367. \tag{40}$$

Then,

$$\boldsymbol{F} = [-\lambda_0] = -367 \quad \text{and} \quad \boldsymbol{g} = 1. \tag{41}$$

In this way, the controller parameters are designed, as well as the internal filters. Therefore, the control law can be defined through (31).

4 Simulation Results

Following are presented the simulations of *tractor* module system controlled by proposed strategy. The simulations were performed with discretisation by *Euler* method and with sampling time equal to $1\,kHz$.

For the discussion of results, simulations were performed for two situations: one with reference application only, and other considering application of disturbance, parametric variation, and process and measurement noises.

Revista Mundi, Engenharia e Gestão, Paranaguá, PR, v. 6, n. 4, p. 374-01, 374-24, 2021.
DOI: 10.21575/25254782rmetg2021vol6n41464

4.1 Reference application

The following simulation was performed only with the application of a reference velocity as a system input, considered equal to $30\,mm/s$, and during $5\,s$. It is emphasised that this is the approximate output value when the system motor receives an armature voltage equal to $12\,V$.

In Figures 6 to 8 are presented the velocity tracking, tracking error and applied control action, respectively. With this control approach, the velocity response y showed a time constant equal to $0.287\,s$ and accommodation time ($2\,\%$) of $0.792\,s$. In that Figure, it is also presented the model reference response y_{mod}, and can be seen that plant output followed reference model output, characteristic of this control strategy. This control action was within the operating voltage limits of the robot, but with a slight overshoot, in the initial transient regime, with voltage equal to $12.35\,V$.

Figure 6: Closed-loop system response: velocity tracking

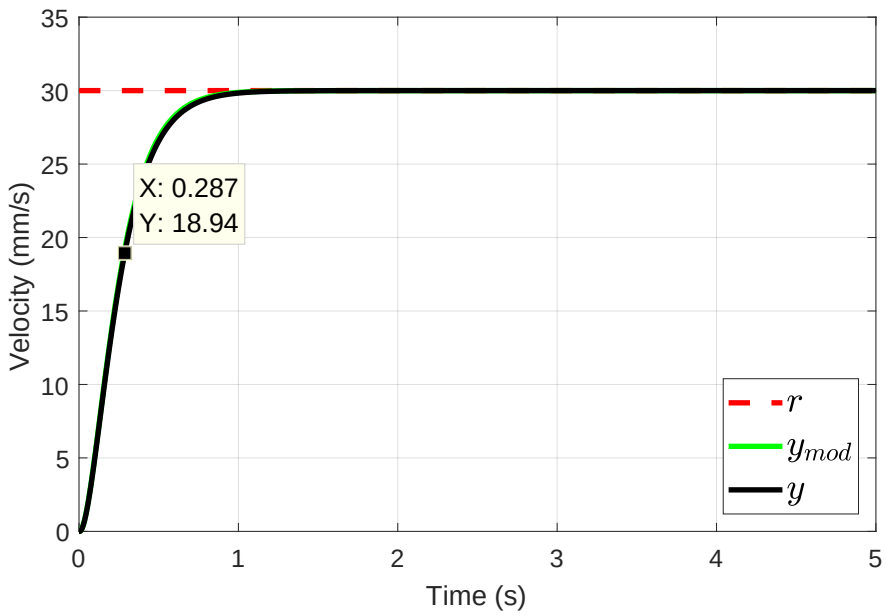

Source: From authors (2021)

4.2 Application of disturbance, parametric variation and noises

The following simulation was also carried out with the application of a reference velocity equal to $30\,mm/s$, but a disturbance, parametric variation and noises were also applied.

The disturbance application corresponds to a change in the disturbance torque

Revista Mundi, Engenharia e Gestão, Paranaguá, PR, v. 6, n. 4, p. 374-01, 374-24, 2021.
DOI: 10.21575/25254782rmetg2021vol6n41464

Figure 7: Closed-loop system response: tracking error

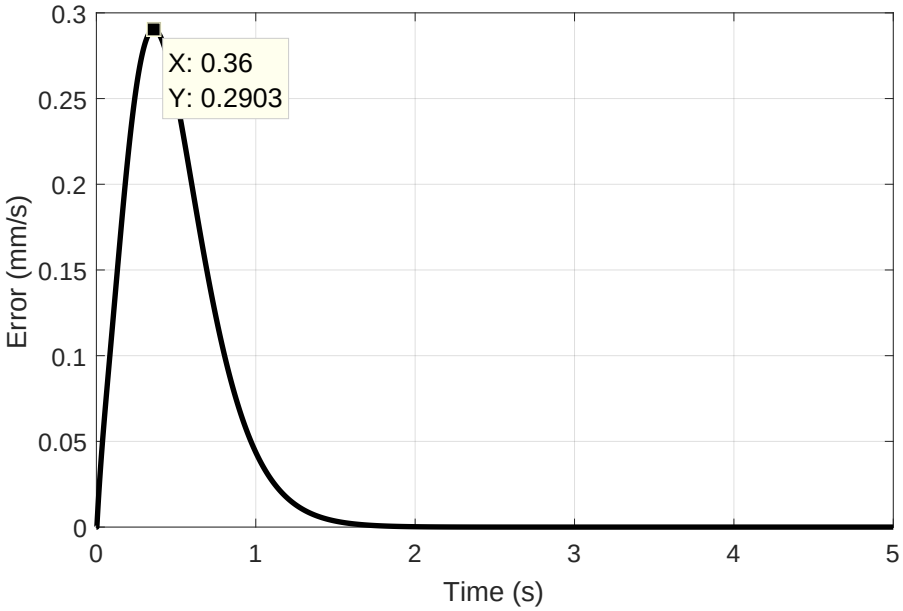

Source: From authors (2021)

Figure 8: Closed-loop system response: control action

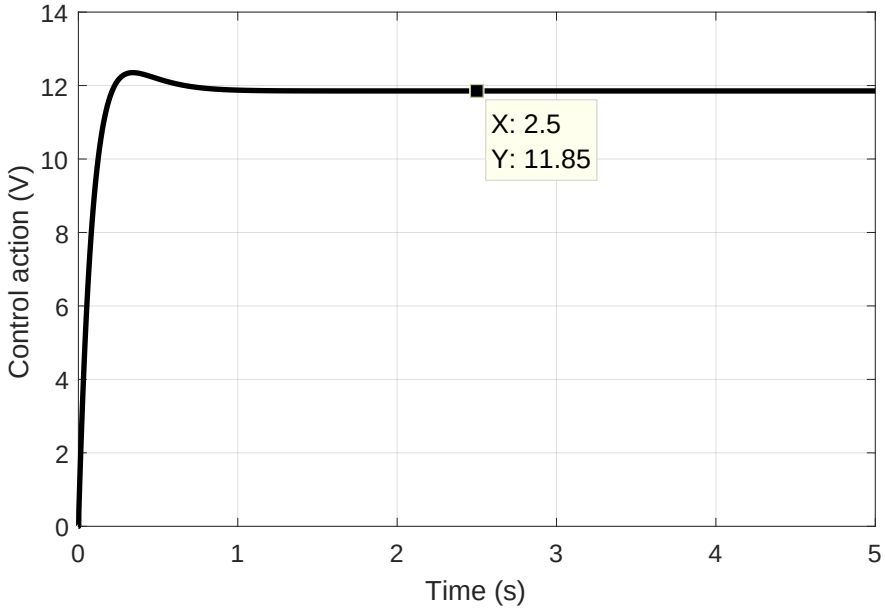

Source: From authors (2021)

value T_d, this value being considered equal to the sixth part of the electromagnetic torque T_e that appears on application of motor's nominal armature voltage ($12\,V$). Besides, the parametric variation corresponds to the application of twice the robot total

Revista Mundi, Engenharia e Gestão, Paranaguá, PR, v. 6, n. 4, p. 374-01, 374-24, 2021.
DOI: 10.21575/25254782rmetg2021vol6n41464

mass, which was originally equal to $11.1\,kg$. Applying this mass to the robot, the viscous friction coefficient also increases, so it has been multiplied by 20 times. This variation was defined with such value that control actions were better perceived. In addition to the disturbance and parametric variation, process and measurement noises were also applied in order to make the simulation closer to the real system. The process noise corresponds to the interference that may arise in the drive system, and was inserted in the simulation added to the armature voltage, that is, the plant input. The measurement noises correspond to variations of velocity measurement. It was inserted in the plant output velocity. The applied noises have random values normalised between -1 and 1, being 65%.

The simulation was carried out during $10\,s$, with the disturbance torque applied at $2\,s$ and removed at $4\,s$. Furthermore, the parametric variation applied at $6\,s$ and removed at $8\,s$. Figures 9 to 11 presents the velocity response, tracking error and control action of closed-loop system with MRC, respectively.

Figure 9: System response with MRC with application of disturbance, parametric variation and noises: velocity tracking

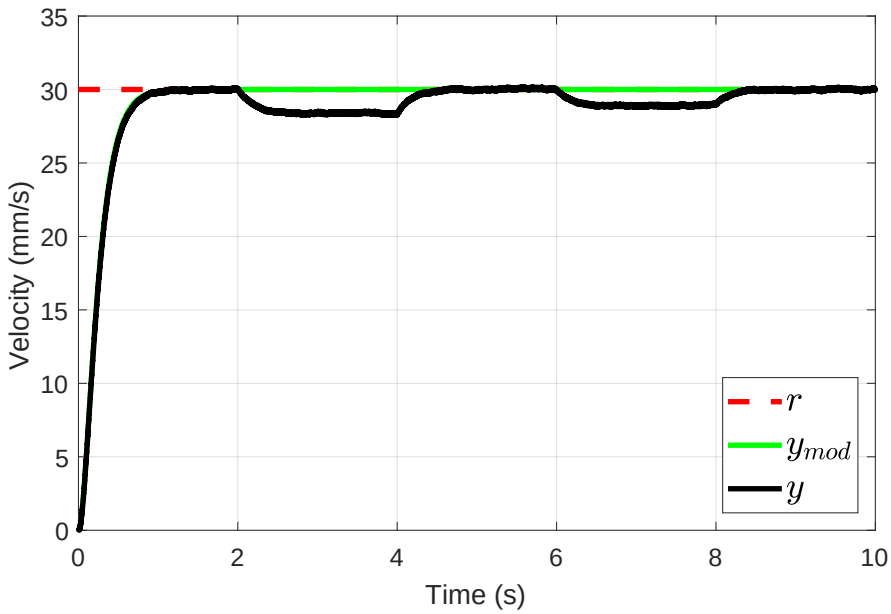

Source: From authors (2021)

The system was affected by variations applied as expected, however, as can be seen, the controller was not able to track the reference properly when subjected to external disturbances and parametric variations, which is its main drawback. This occurred because this control technique considers a credible model of the plant,

Revista Mundi, Engenharia e Gestão, Paranaguá, PR, v. 6, n. 4, p. 374-01, 374-24, 2021.
DOI: 10.21575/25254782rmetg2021vol6n41464

Figure 10: System response with MRC with application of disturbance, parametric variation and noises: tracking error

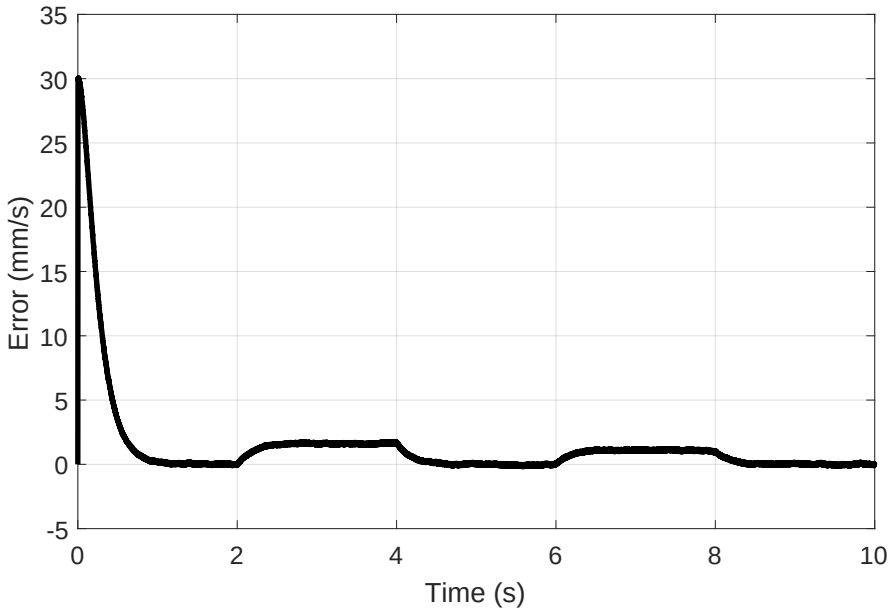

Source: From authors (2021)

Figure 11: System response with MRC with application of disturbance, parametric variation and noises: control action

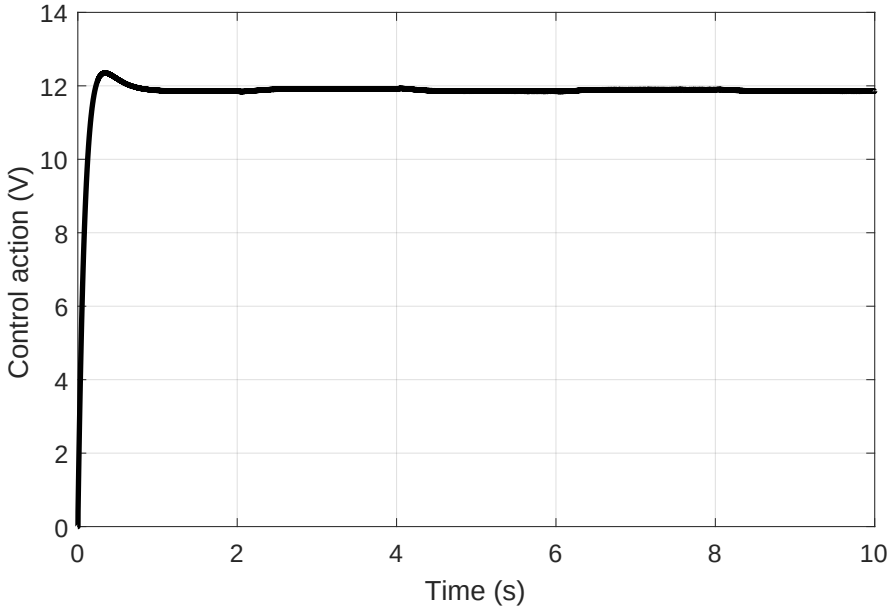

Source: From authors (2021)

and, when plant is affected by parametric variations or subjected to relevant external unmodelled disturbances, the controller is not able to track the desired reference. To

Revista Mundi, Engenharia e Gestão, Paranaguá, PR, v. 6, n. 4, p. 374-01, 374-24, 2021.
DOI: 10.21575/25254782rmetg2021vol6n41464

get around this problem, it is necessary for the controller to consider adapting its gains and robustness techniques, which we intend to implement in a future work. Back in MRC performance analysis, the maximum error displayed by controller, was observed during the disturbance application, with $1.06\,mm/s$.

5 Experimental Results

After the simulations, an experiment was carried out. The control action was synthesised using a microcontroller. It is worth mentioning that, in practice, the control action represents a PWM (Pulse Width Modulation) signal applied to the motor pins. The discretisation of the equations was also performed by *Euler* method with a discretisation time equal to $1\,kHz$.

The experiment was carried out for situation with application of a reference velocity equal to $30\,mm/s$, without inserting disturbances. Then, it was realised that, with gains considered on simulations, a velocity response was not possible. Thus, the $\boldsymbol{F}$ matrix had its value changed from -367 to -355.5, obtaining a velocity response, which is shown on Figure 12. The adjusted response showed a constant time and accommodation time equal to $0.650\,s$ and $2.068\,s$, respectively. It is emphasised that marker in the Figure corresponds to the accommodation time (2%).

Figure 12: Experimental system velocity response with MRC controller

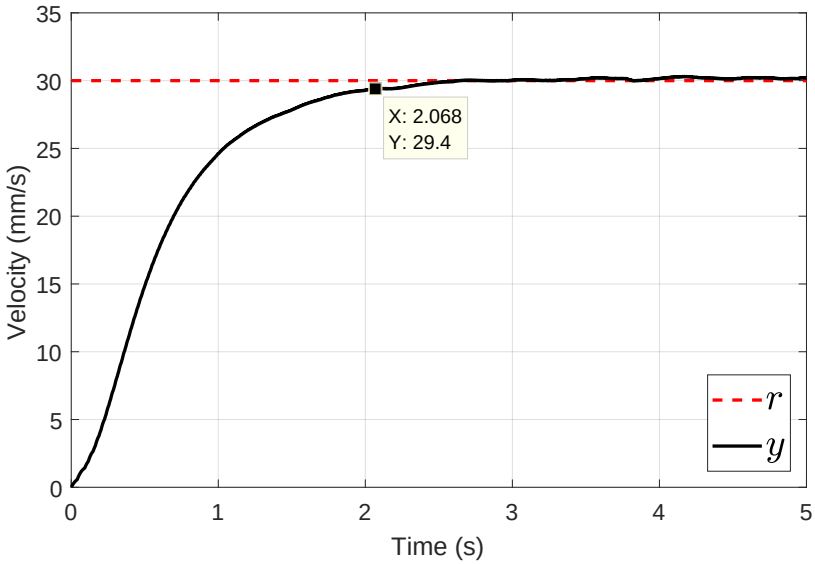

Source: From authors (2021)

The Figure 13 presents experimental error of the velocity tracking. It is

Revista Mundi, Engenharia e Gestão, Paranaguá, PR, v. 6, n. 4, p. 374-01, 374-24, 2021.
DOI: 10.21575/25254782rmetg2021vol6n41464

emphasised that data referring to the control action was not collected due to memory limitations of the microcontroller. However, once tracking error converges asymptotically to zero, and there were no oscillations on tracking reference, it means that voltage source was enough to supply the required control action.

Figure 13: Experimental system error with reference equal to $30\,mm/s$

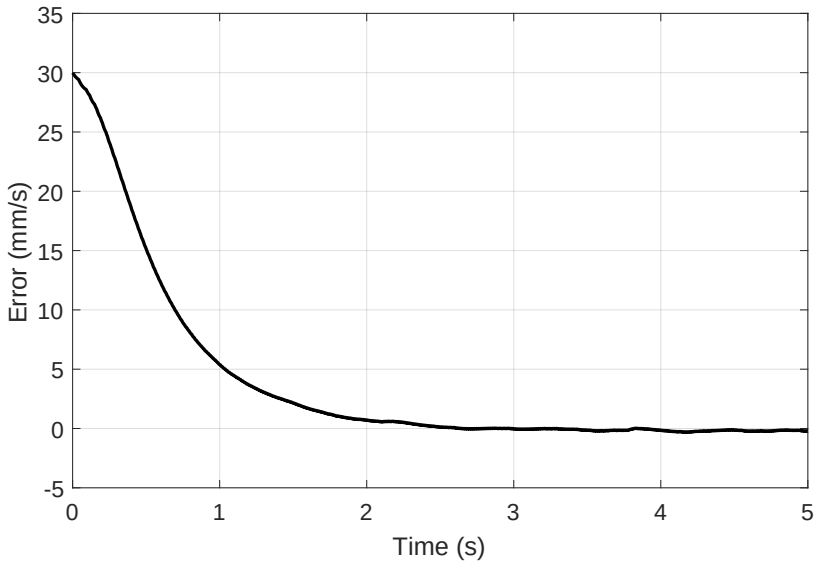

Source: From authors (2021)

6 Conclusion

This work presented the application of Model Reference Control strategy in a welding robot. For this, robot modelling was briefly presented and control theory of MRC was explained. Finally, simulation and experimental results were presented that proved the potentiality of applying this technique in velocity tracking of the robot. It can be observed that system reached the reference value, at approximately $1\,s$, maintaining a null stationary error and following reference model output. When subjected to disturbances, parametric variations and noises, the plant output presented a response with variations. However, the plant, after each change, was able to return to its reference value. Thus, it is concluded that MRC presented satisfactory results, being an adequate choice for velocity control of the welding robot. In addition, it is emphasised that variations perceived in the system curves, when submitted to changes, can be controlled using adaptive MRC, such as Model Reference Adaptive Control (MRAC) and Robust Model Reference Adaptive Control (RMRAC).

Revista Mundi, Engenharia e Gestão, Paranaguá, PR, v. 6, n. 4, p. 374-01, 374-24, 2021.
DOI: 10.21575/25254782rmetg2021vol6n41464

References

BUG-O SYSTEMS CORPORATION. *Catalog of the Modular Drive System*. 1. ed. Canonsburg, PA, 2019. P. 1–16. 4

BUG-O SYSTEMS CORPORATION. *Instructions and parts manual: modular drive system*. 1. ed. Canonsburg, PA, 2019. P. 1–60. 4

CHEN, S. J. et al. Machine-assisted travel speed control in manual welding torch operation. *The International Journal of Advanced Manufacturing Technology*, Springer, v. 76, n. 5, p. 1371–1381, 2015. 2

CORREIA, F. et al. Correlação entre a velocidade de soldagem e da alimentação do arame no processo de soldagem gmaw com a geometria, microestrutura e macroestrutura do cordão de solda. *22º CBECiMat - Congresso Brasileiro de Engenharia e Ciência dos Materiais*, 2016. 2

DECANIO, S. J. Robots and humans–complements or substitutes? *Journal of Macroeconomics*, Elsevier, v. 49, p. 280–291, 2016. 2

DECKER, M.; FISCHER, M.; OTT, I. Service robotics and human labor: A first technology assessment of substitution and cooperation. *Robotics and Autonomous Systems*, Elsevier, v. 87, p. 348–354, 2017. 2

FERREIRA, A. S. R. et al. Displacement velocity control of a mechanised welding system by low-cost state feedback controller. *International Journal of Modelling, Identification and Control*, Inderscience Publishers (IEL), v. 36, n. 2, p. 136–144, 2020. 5

IOANNOU, P. A.; SUN, J. *Robust adaptive control*. [S.l.]: PTR Prentice-Hall Upper Saddle River, NJ, 1996. 8, 11, 14

LIU, Y.; ZHANG, Y. Fusing machine algorithm with welder intelligence for adaptive welding robots. *Journal of Manufacturing Processes*, Elsevier, v. 27, p. 18–25, 2017. 2

MARK, M. van der et al. Occupational exposure to solvents, metals and welding fumes and risk of parkinson's disease. *Parkinsonism & related disorders*, Elsevier, v. 21, n. 6, p. 635–639, 2015. 2

MENDES, C. et al. Estudo da influência da velocidade de soldagem na tensão residual de juntas soldadas pelo processo gmaw. *22º CBECiMat - Congresso Brasileiro de Engenharia e Ciência dos Materiais*, 2016. 2

MISTRY, P. K. J. Impact of welding processes on environment and health. *International Journal of Advanced Research in Mechanical Engineering & Technology*, p. 17–20, 2015. 2

NATHAN, S. R. et al. Effect of welding processes on mechanical and microstructural characteristics of high strength low alloy naval grade steel joints. *Defence Technology*, Elsevier, v. 11, n. 3, p. 308–317, 2015. 2

SINGH, Z.; CHADHA, P. Assessment of dna damage as an index of genetic toxicity in welding microenvironments among iron-based industries. *Toxicology and industrial health*, SAGE Publications Sage UK: London, England, v. 32, n. 10, p. 1817–1824, 2016. 2

ÜNEL, E.; TABAN, E. Properties and optimization of dissimilar aluminum steel cmt welds. *Welding in the World*, Springer, v. 61, n. 1, p. 1–9, 2017. 2

YUXIANG, H.; DONG, D.; JILUAN, L. X. P. Seam-tracking based on dynamic trajectory planning for a mobile welding robot. *China Welding*, v. 28, n. 4, p. 46–50, 2019. 2

Enviado em: 05 nov. 2020.

Aceito em: 25 nov. 2021.

Editora responsável: Bianca Neves Machado.